IEEE Access
Multidisciplinary | Rapid Review | Open Access Journal

SPECIAL SECTION ON BATTERY ENERGY STORAGE AND MANAGEMENT SYSTEMS

Received December 4, 2017, accepted December 14, 2017, date of publication December 18, 2017,
date of current version February 14, 2018.

Digital Object Identifier 10.1109/ACCESS.2017.2784836

Handling Stability Improvement for a Four-Axle Hybrid Electric Ground Vehicle Driven by In-Wheel Motors

MINGCHUN LIU, JUHUA HUANG, AND MING CAO
School of Mechatronics Engineering, Nanchang University, Nanchang 330031, China

Corresponding author: Mingchun Liu (liumingchun@ncu.edu.cn)

This work was supported in part by the National Natural Science Foundation of China under Grant 51605214 and in part by the Natural Science Foundation of Jiangxi Province under Grant 20171BAB216028.

ABSTRACT The hybrid electric ground vehicle (HEGV), driven by in-wheel motors (IWMs), is a good solution for prolonging vehicle driving range and improving dynamics performance. This paper presents a hierarchical optimization control strategy for a four-axle HEGV driven by IWMs to improve handling stability. In the proposed hierarchical control strategy, the upper layer controller controls the vehicle motion states to track the desired ones, in which the controlled force and moment are considered as resultant of the longitudinal tire force, and is determined by using the nonlinear sliding mode control method. In the lower layer controller, the control allocation method is adopted to assign torque to all actuators, including the IWMs and brakes, to generate the controlled force and moment determined by the upper layer controller. Considering the motor torque capability, tire workload rate, and road adhesion, we establish an objective function with constraints, which is solved by using the optimization algorithm. The software simulation and the hardware-in-loop test results show that the proposed control strategy exhibits excellent performance in terms of vehicle handling stability, compared with the commonly used control strategies, and has the capability of real-time implementation.

INDEX TERMS Control allocation, four-axle ground vehicle, hybrid electric vehicle, in-wheel motor, sliding mode control, vehicle handling stability.

I. INTRODUCTION

Vehicle electrification is a current and future direction in the automotive industry. Compared to Pure Electric Vehicles (PEVs), which are hampered by battery technology due to limited range and lengthy charge times, the Hybrid Electric Vehicles (HEVs) have the potential to bridge the gap between the conventional Internal Combustion Engine (ICE) powered vehicles and the PEVs [1], [2]. In some special purposes and military fields, the multi-axle Hybrid Electric Ground Vehicles (HEGVs) have been developed for improving energy efficiency and driving range [3], [4]. Most researchers have concentrated on the power management strategy of HEVs [5]–[9]. The majority of driving conditions of multi-axle ground vehicles include high speeds with heavy loads, drastic turning maneuvers, and on slippery roads [10]. Appropriately equipping the stability control systems for multi-axle HEGVs is necessary.

With the development of In-Wheel Motors (IWMs), compared to the HEGVs driven by centralized motors, the HEGVs driven by IWMs, as shown in Fig. 1, have great potential to improve vehicle handling stability and dynamics performance. That is because the IWMs, which are mounted into wheel hubs, can be independently controlled and directly actuated. The redundancy and flexibility of

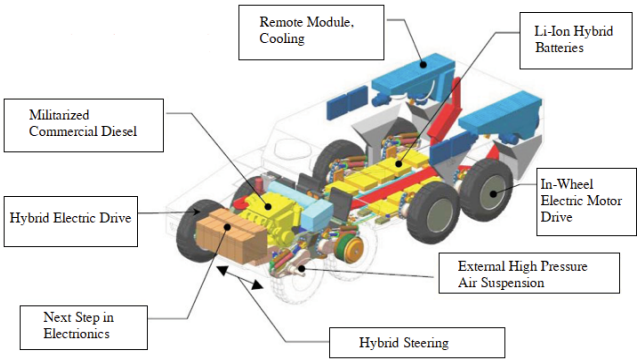

FIGURE 1. Hybrid electric ground vehicle driven by in-wheel motors.

IWMs reinforce the performance of vehicle dynamics control. In addition, the removing centralized powertrains is beneficial to design vehicle weight distribution for best handling performance [11]–[14]. However, these merits are companied with technical challenges. The usage of IWMs alters vehicle structural and mechanical parameters. Vehicle dynamics characteristics are significantly changed, so that the existing vehicle dynamics control systems are not well applicable. What is more, the redundant IWMs perform as an over-actuated system with complicated constrains. Especially for the multi-axle HEGVs driven by IWMs, the coordinated torque allocation among multiple IWMs is crucial to improve vehicle handling stability.

Various methods for improving handling stability have been studied and actively developed for two-axle vehicles driven by IWMs, and studies of multi-axle vehicles have been conducted based on those findings. These methods mainly focus on vehicle motion control and driving/braking torque allocation. Hierarchical and centralized control strategies are used in vehicle dynamics control, and the hierarchical control strategy has been proved to be more flexible and effective [15]. In a hierarchical strategy, the upper layer is considered as a vehicle motion controller to maintain vehicle dynamics stability by determining the desired force and/or moment, and the lower layer serves as a torque allocation controller in charge of assigning force and torque to each actuating motor and/or brake to generate the desired force and/or moment required by the upper layer [16].

In vehicle motion control research, vehicle yaw rate and side slip angle, based on the two degrees of freedom (DOFs) linear model, are generally considered as vehicle desired motion states [17] because most drivers are familiar with vehicle dynamics performance and able to control vehicle with stability in the linear region of the vehicle. In addition, the desired yaw rate and side slip angle are constrained by the road adhesion conditions and vehicle stability margin [18], [19]. By linearizing the tire dynamics model, the vehicle yaw rate and side slip angle can be synchronously controlled based on linear control methods [20], which can improve vehicle stability in the linear region of the tire. However, tires have nonlinear characteristics under the high speed and low adhesion conditions, which weakens the effectiveness of the linear control methods. Therefore, nonlinear control methods are adopted to handle the nonlinear characteristics of the vehicle and tire. Chen *et al.* [12] considered the yaw rate and the side slip angle as an interacting system with nonlinear characteristics. They set the yaw rate as an intermediate variable, and controlled the side slip angle by using the dynamic sliding mode control (SMC) method to improve vehicle handling stability.

In addition, various nonlinear adaptive control methods, such as the neural network control method [21] and fuzzy control method [22], are widely used to determine the desired force and/or moment for maintaining vehicle motion stability. However, as indicated in [12], the yaw rate interacts with the side slip angle, meaning they are not independently controlled to track the desired states with a single control variable, such as the desired force or desired yaw moment. The integrated control method [23], based on the active steering control and the direct yaw-moment control (DYC), is effective for independently controlling the yaw rate and side slip angle. However, it is not applicable to vehicles without active steering equipment.

In the torque allocation research, the driving and/or braking torque is assigned to actuators, such as IWMs and brakes, by using the rules-based methods or optimization-based methods. Jackson *et al.* [24] established 49 fuzzy rules, based on the yaw rate and the change rate of a three-axle HEGV driven by IWMs, to allocate the driving torque of the six IWMs. Wang textitet al. [25] assigned the torque to the two-side tires based on the rules of equal values and opposite directions. The rule-based control methods are effective but lack of accuracy and optimality, resulting in a suboptimal performance. The optimization-based method, by contrast, can simultaneously handle multiple control objectives and actuator constraints, and can perform actuator reconfiguration, to some extent, when encountering issues such as actuator failures [16], [26].

Kyongsu [10], [27] investigated the optimal torque allocation for three-axle and four-axle HEGVs driven by IWMs, in which the objective functions were established based on the yaw rate and the tire load rate. The Generalized Inverse Method (GIM) and a numerical algorithm of extremum were used to solve the objective functions to calculate the optimal torque allocation. Wang *et al.* [28] proposed a real-time hierarchical control algorithm for a multi-axle land vehicle with IWMs to improve the vehicle performance, in which an optimal control allocation algorithm was adopt to coordinate the motor torque under some physical constraints of the actuators and the tire dynamics. Zhao *et al*. [29] investigated a nonlinear control allocation scheme, based on the model predictive control (MPC) method, for EVs with IWMs to improve vehicle stability, in which the constraints of actuating motors and tire slip ratio were considered to address the unintended side effects, such as skidding or discomforting the driver under critical driving conditions. Xiong *et al.* [30] proposed a direct yaw control method, based on driver operation intention, for stability control of an EV driven by IWMs under emergency steering alignment conditions. The driving conditions could be identified by using the driver operation intention recognition module, and the motor torque is optimally allocated by using an active set algorithm. Novellis *et al*. [31] established different objective functions and constraints based on the motor performance, the battery capacity, and the road adhesion, and the optimal torque allocation was found by using an interior point algorithm.

According to these studies, torque can be precisely allocated by using the optimization algorithm with simplified constraints. However, the optimization accuracy would decrease under complex conditions, meanwhile, the reliability and real-time performance need to be improved. In addition, most of the studies were conducted on two-axle vehicles.

Whereas, the motion control and torque allocation are much more complicated for a vehicle with more axles.

To address these drawbacks in vehicle motion control and torque allocation for multi-axle HEGV driven by IWMs, this study proposes an optimization control strategy with hierarchical structure to improve vehicle handling stability. The main contributions lie in the following aspects. First, the upper layer controller, by using the sliding mode control (SMC) method, is devised to determine the controlled force and yaw moment to ensure vehicle motion states track the desired states for motion stability, whereby the vehicle velocity, yaw rate, and side slip angle are independently controlled. Second, in the lower layer controller, by using the control allocation (CA) method, the driving and braking torque are assigned to all actuators, including the IWMs and brakes. We consider the motor capacity and tire adhesion as constrains, and establish an objective function based on the tracking precision and tire workload rate to optimize the torque allocation on the eight IMWs and eight brakes. Finally, a simulation based on the Matlab/Simulink software, and a test experiment based on the controller hardware-in-loop (HIL) platform, are conducted to validate the effectiveness of the proposed control strategy.

The remaining sections of this paper are organized as follows. Section II introduces the architecture and nonlinear dynamics model of a four-axle HEGV driven by IWMs. A hierarchical control strategy for improving vehicle handling stability is explained in Section III. The software simulation and the HIL test results of the proposed control strategy are demonstrated in Section IV. Finally, the conclusions are drawn in Section V.

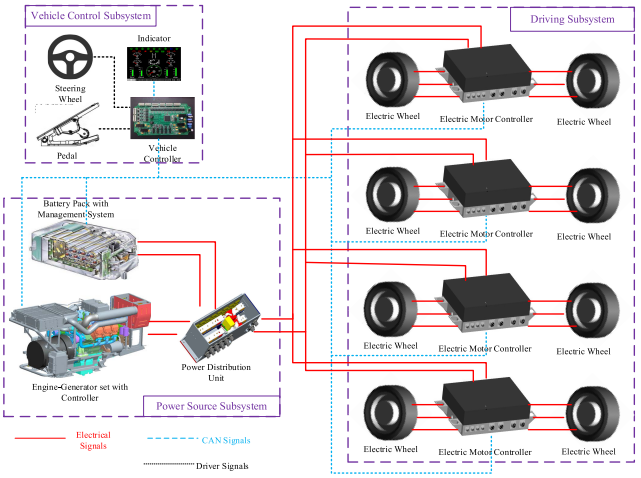

FIGURE 2. Architecture of a four-axle HEGV driven by IWMs.

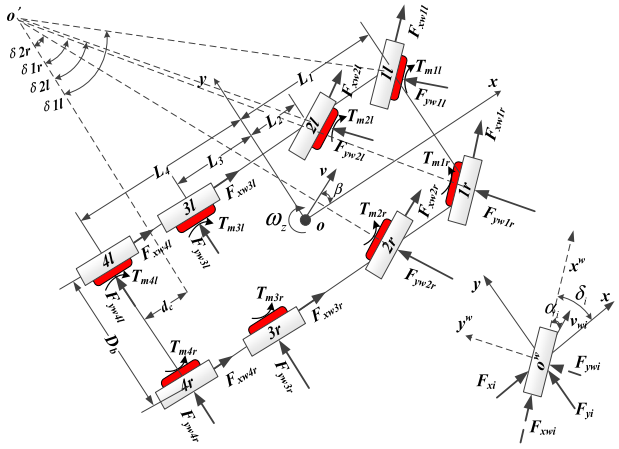

FIGURE 3. Vehicle system dynamics model.

II. VEHICLE SYSTEM DYNAMICS MODELING

A. VEHICLE ARCHITECHURE DESCRIPTION

The architecture of a four-axle HEGV driven by IWMs is shown in Fig. 2, with three subsystems: the vehicle control subsystem, the hybrid power source subsystem, and the electric driving subsystem. The vehicle control subsystem communicates with other subsystems through the Controller Area Network (CAN) bus, sending control signals and receiving feedback signals. The hybrid power source is mainly composed of a power battery pack and an engine-generator set with their management systems. The electric power of the battery and that of engine-generator set converges and then the power is distributed to the electrical components by the power distribution unit. The electric driving subsystem consists of the IWMs and their controllers. Each controller can independently control the tow coaxial motors, and each motor is mounted into the wheel hub with a wheel-side reducer.

B. VEHICLE SYSTEM DYNAMICS MODEL

To improve vehicle handling stability, we primarily focus on the control of vehicle planar motion. Regardless of the influences of suspension system, we assume that the vehicel is driven on a flat surface by eight IWMs. The vehicle system model, as shown in Fig. 3, has 11 free degrees of freedom (DOFs), including 3 DOFs of vehicle planar motion (longitudinal, lateral, and yaw motions) and 8 DOFs of wheel rotational motion. To clearly state the model, the subscripts i and j ($i = 1, 2, 3, 4$; $j = r, l$) are used to denote the wheel numbers. For example, the subscript $1l$ denotes the left wheel in first axle.

According to the force equilibrium and the moment balance on the vehicle coordinate frame (o-xyz) with the origin located at the center of gravity (C.G.), the dynamics equations of vehicle model in Fig. 3 can be expressed as:

$$m(\dot{v}_x - v_y\omega_z) = \sum_{i=1}^{4}(F_{xil} + F_{xil}) - (mgf_r + 0.5C_DA_f\rho_a v_x^2) \tag{1}$$

$$m(\dot{v}_y + v_x\omega_z) = \sum_{i=1}^{4}(F_{yil} + F_{yil}) \tag{2}$$

$$I_z\dot{\omega}_z = \frac{D_b}{2}\sum_{i=1}^{4}(F_{xir} - F_{xil}) + \sum_{i=1}^{2}[L_i(F_{yil} + F_{yir})] - \sum_{i=3}^{4}[L_i(F_{yil} + F_{yir})] \tag{3}$$

where m and I_z represent the vehicle mass and vehicle yaw inertia, respectively;v_x, v_y, and ω_z represent the vehicle longitudinal velocity, lateral velocity, and yaw rate, respectively. L_i (i = *1, 2, 3, 4*) represents the distance from each axle to the C.G.. And $D_b$is the wheelbase between the left and right wheels. F_{xij} and F_{yij} (i = *1, 2, 3, 4*; j=*r,l*) represent the longitudinal tire force and lateral tire force on the vehicle coordinate frame (o-xyz), respectively; g represents the gravity acceleration. f_r represents the rolling resistance coefficient. C_D presents the drag coefficient. A_f presents the vehicle frontal area, and ρ_a presents the air density.

The longitudinal tire force and lateral tire force are basically measured on the tire coordinate frame (o^w-$x^w y^w z^w$) with the origin located at the tire center. The relationship between the tire force in the vehicle coordinate frame and that in the tire coordinate frame can be expressed as:

$$\begin{cases} F_{xij} = F_{xwij}\cos\delta_{ij} - F_{ywij}\sin\delta_{ij} \\ F_{yij} = F_{xwij}\sin\delta_{ij} + F_{ywij}\cos\delta_{ij} \end{cases} \tag{4}$$

where F_{xwij} and F_{ywij} (i = *1,2,3,4*; j=*r,l*) represent the longitudinal tire force and lateral tire force on the tire coordinate frame (o^w-$x^w y^w z^w$), respectively; and δ_{ij}(i = *1,2,3,4*; j=*r, l*) presents the steering angle of each wheel. In this paper, the vehicle is steered with the front two axles, thus δ_{ij} (i = *3, 4*; j=*r, l*) = 0. The four front wheels steering angles can be derived as:

$$\begin{cases} \delta_{1l} = \dfrac{\delta_{sw}}{i_{sw}} \\ \delta_{2l} = \operatorname{arc\,cot}\left(\dfrac{L_1 + L_4 - d_c}{L_2 + L_4 - d_c} \cdot \cot\delta_{1l}\right) \\ \delta_{1r} = \operatorname{arc\,cot}\left(\dfrac{D_b}{L_1 + L_4 - d_c} + \cot\delta_{1l}\right) \\ \delta_{2r} = \operatorname{arc\,cot}\left(\dfrac{D_b}{L_2 + L_4 - d_c} + \dfrac{L_1 + L_4 - d_c}{L_2 + L_4 - d_c} \cdot \cot\delta_{1l}\right) \\ d_c = \dfrac{L_4 - L_3}{2} \end{cases} \tag{5}$$

where δ_{sw} represents the steering wheel angle, and i_{sw} is the transmission ratio of steering mechanism. In addition, ignoring the wheel vertical movement, the wheel rotational motion can be expressed as:

$$I_{wij}\dot{\omega}_{wij} = T_{wheelij} - T_{fij} - F_{xwij}R_{wij} \tag{6}$$

where I_{wij} represents the wheel rotation inertia; ω_{wij} represents the wheel rotation speed. $T_{wheelij}$ represents the driving force or braking force of the IWM and/or braking system. T_{fij} represents the wheel rolling resistance torque, and R_{wij} is the wheel effective radius.

C. TIRE MODEL

Tire force is crucial to vehicle dynamics control. Especially in the extreme circumstances, such as steering on the slippery road with high speed, nonlinear tire characteristics significantly influence the driving stability. Therefore, building a precise tire model to calculate tire force is necessary. The "Magic Formula" tire model, developed by Jansen *et al.* [32] and Bakker *et al.* [33], is widely used in vehicle dynamics research, and can accurately calculate the longitudinal tire force and lateral tire force based on the basic parameters, and is adopted in this study.

The magic formula is a type of mathematical formula that is capable of describing basic tire characteristics surprisingly. Under pure longitudinal slip circumstances, the longitudinal tire force can be expressed as a function based on the vertical load and the longitudinal slip ratio. Under pure lateral slip conditions, the lateral tire force can be expressed as a function based on the vertical load and the lateral slip angle. The basic magic formula of the tire model can be expressed as:

$$y(x) = D\sin\{C\arctan[Bx - E(Bx - \arctan(Bx))]\} \tag{7}$$

where y represents the longitudinal tire force or lateral tire force in the pure slip circumstances. x represents the longitudinal slip ratio or lateral slip angle of tire. *B, C, D,* and E are the performance parameters based the testing data.

Further, under combined slip circumstances, the tire is driven or braked while it is cornering. Based on the "magic formula", the tire force is fitted with the weighting functions as follows:

$$\begin{cases} F_x = F_{x0} \cdot G_{x\alpha}(\alpha, \lambda, F_z) \\ F_y = F_{y0} \cdot G_{y\lambda}(\alpha, \lambda, F_z) \end{cases} \tag{8}$$

where F_x and F_y represent the longitudinal tire force and lateral tire force in the combined slip circumstances, respectively. And F_{x0} and F_{y0} represent the longitudinal tire force and lateral tire force in the pure slip circumstances, respectively. $G_{x\alpha}$ and $G_{y\lambda}$ represent the weighting functions.

In this paper, the longitudinal tire force and lateral tire force under pure slip conditions with different road adhesion coefficients are shown in Fig. 4(a) and (b), respectively. The longitudinal tire force and lateral tire force in combined slip conditions are shown in Fig. 4(c).

D. IN-WHEEL MOTOR MODEL AND ELECTRIC WHEEL TORQUE REGULATION

In this paper, eight permanent magnet synchronous motors (PMSMs) with inner rotor are assembled into the hubs. In each electric wheel, a reducer is connected to the inner rotor to increase the driving torque. To satisfy the power performance of the four-axle ground vehicle, a PMSM featuring a peak torque of 1100Nm and a peak power of 90kW is selected. Based on bench testing data, a lookup table-based model of the PMSM, as shown in Fig. 5, is introduced. The PMSM model considers the motor torque coefficient and rotation speed as inputs, and the motor torque as an output. The introduced lookup-table model can be simply expressed as:

$$T_{mij} = f(a_{ij}, n_{ij}) \tag{9}$$

where T_{mij} represents the PMSM torque. a_{ij} represents the torque coefficient and $-1 \le a_{ij} \le 1$. n_{ij} represents the PMSM

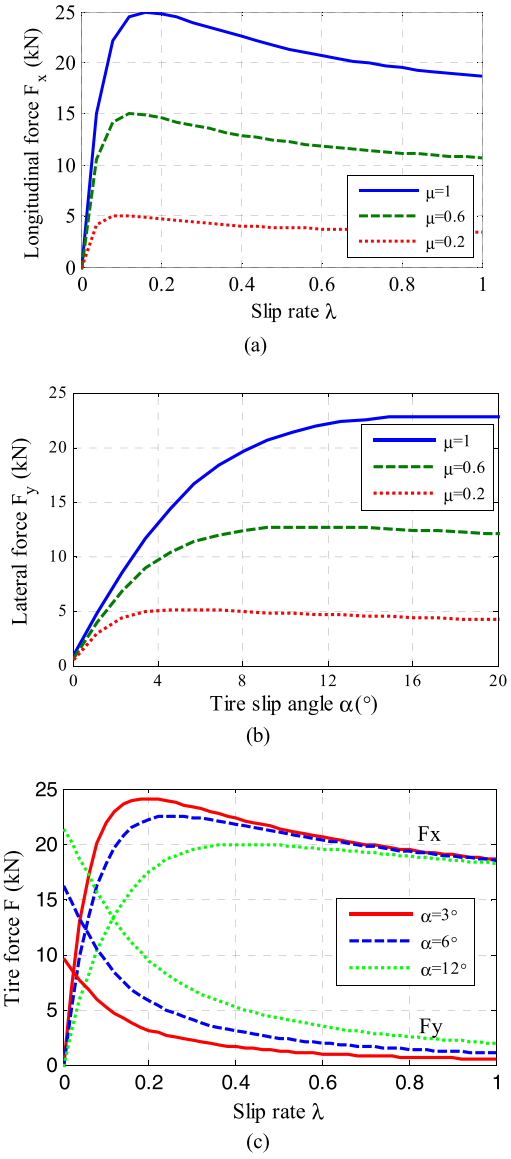

FIGURE 4. Tire forces based on the "magic formula" tire model. (a) Tire longitudinal force under pure longitudinal slip conditions. (b) Tire lateral force under pure lateral slip conditions. (c) Tire forces under combined slip conditions.

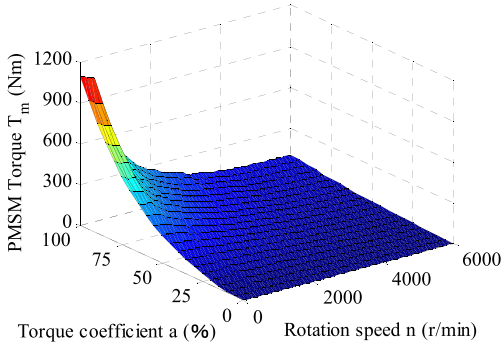

FIGURE 5. Lookup table-based model of the PMSM.

rotation speed, and f () represents the lookup-table function based on the testing data.

The torque actuators in each electric wheel include a PMSM and a brake. The effective torque acting on the wheel includes the PMSM torque and braking system torque, so the PMSM can provide both driving and braking torque, and the braking system can provide braking torque only. Therefore, the effective torque acting on the wheel is limited due to the capacity of PMSMs and braking system, as shown in Fig. 6.

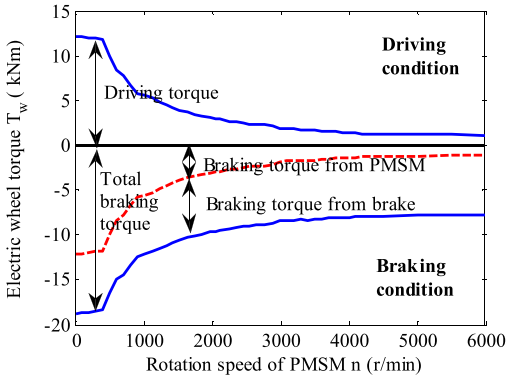

FIGURE 6. Effective torque limitation of electric wheel.

When driving, the effective torque of electric wheel only originates from the PMSM, and can be expressed as:

$$T_{wij} = T_{mij} \cdot i_g \tag{10}$$

where T_{wij} represents the effective torque acting on the wheel, and i_g represents the transmission ratio of the wheel-side reducer.

When braking, we assumed that the effective torque of electric wheel primarily originates from the PMSM, and the mechanical braking system is considered as a supplement. That can be expressed as:

$$T_{wij} = \begin{cases} -T_{mij} \cdot i_g, & if \ \left|T_{wij}\right| \le T_{\max mij} \cdot i_g \\ -T_{\max mij} \cdot i_g - T_{bij}, & if \ \left|T_{wij}\right| > T_{\max mij} \cdot i_g \end{cases} \tag{11}$$

where the minus sign denotes that the wheel is working under the braking conditions. T_{maxmij} is the maximum PMSM torque responding to its rotation speed. T_{bij} is the mechanical braking system torque.

III. VEHICLE HANDLING STABILITY CONTROL STRATEGY

A. HIERARCHICAL CONTROL SCHEME

Vehicle handling stability can be evaluated based on the key motion states, the longitudinal velocity, side slip angle, and yaw rate. According to the vehicle dynamics model, the three key states can be controlled by the resultant force and yaw moment acting on vehicle body. The controlled force and yaw moment are the resultant of the tire force. Furthermore, the tire force originates from the IWMs torque and braking system torque.

In this study, the vehicle motion control and the actuator torque allocation are processed in different layers in a hierarchical scheme. And a hierarchical control strategy is proposed to address the dynamics coupling and nonlinear issues, as shown in Fig. 7. In the proposed strategy, the desired motion

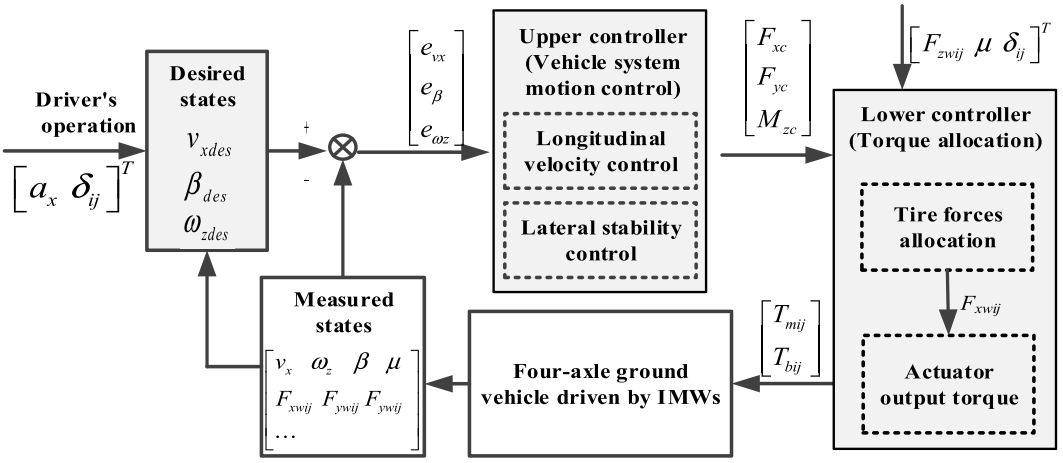

FIGURE 7. Vehicle handling stability control strategy with hierarchical structure.

states include the desired longitudinal velocity v_{xdes}, desired side slip angle β_{des}, and desired yaw rate ω_{zdes}. To eliminate the biases between the measure states and desired states, an upper layer controller is designed to calculate the controlled resultant force and yaw moment acting on the vehicle body, whereby a controlled longitudinal force F_{xc}, a controlled lateral force F_{yc}, and a controlled yaw moment M_{zc} can independently control the longitudinal velocity, side slip angle, and yaw rate, respectively. The lower layer controller is designed to calculate the driving and braking torque of each actuator, including the IWM and braking system, to satisfy the controlled force and moment determined by the upper controller. In addition, we assume that the motion states, such as the velocity and force, can be accurately measured.

B. DESIRED STATES

The desired motion states, i.e., the desired longitudinal velocity, desired side slip angle, and desired yaw rate, are calculated based on the driver's operation and vehicle motion states. The driver provides an acceleration and a steering angle to the vehicle. Based on that, the vehicle motion states are controlled to track the desired states. To enhance vehicle stability, we determine the desired states in the linear manoeuver region of the tire dynamics characteristics.

According to driver's pedal operation, the desired longitudinal velocity can be calculated as:

$$v_{xdes} = v_{x0} + \int_{t_0}^{t} a_x(\tau) d\tau \tag{12}$$

where v_{x0} represents the longitudinal velocity at time t_0, and a_x represents the acceleration command which is assumed to be linear with the pedal angular displacement.

The desired yaw rate is calculated based on the two DOFs linear vehicle model and the road adhesion conditions. The yaw rate under the steady-state steering condition can be calculated as:

$$\omega_{zss} = G_{\omega_z ss} \cdot \delta_1 \tag{13}$$

where $G_{\omega_z ss}$ represents the steady gain of the yaw rate, and δ_1 represents the steering angle of the first axle.

In addition, the yaw rate is limited due to the tire-road adhesion capacity. That is:

$$|\omega_z| \leq \mu \cdot g / v_x \tag{14}$$

where μ represents the tire-road adhesion coefficient. Thus, the desired yaw rate is determined by:

$$\omega_{zdes} = \min(\left|G_{\omega_z ss} \cdot \delta_1\right|, \quad \mu \cdot g / v_x) sgn(\delta_1) \tag{15}$$

A modest side slip angle provides a proper feedback to drivers, whereas the increased side slip angle, especially when the side slip angle exceeds four degrees on slippery roads, leads to a vehicle deviation problem, making the driver feel nervous and vehicle unstable. Therefore the purpose of side slip control is to minimize the side slip angle both in steady and transient states [34], [35]. Two methods are mainly utilized to determine the desired side slip angle. One method is setting the desired side slip to zero to achieve a good performance in trajectory tacking and driver maneuverability. This method is widely adopted in the all-wheel-steering vehicle control [36]–[38]. But for the vehicle without all-wheel-steering function, the lateral force acting on vehicle is inadequate to maintain the zero side slip angle. Thus the other method is calculating the desired side slip angle based on the two DOFs linear vehicle model, meanwhile the desired value is limited due to the tire-road adhesion capacity [39], [40]. That is:

$$\beta_{des} = \min\left[\left|G_{\beta ss} \cdot \delta_1\right|, \quad \arctan(0.02\mu g)\right] \cdot \mathrm{sgn}(\delta_1) \tag{16}$$

where $G_{\beta ss}$ represents the steady gain of the side slip angle. The $G_{\omega_z ss}$ and $G_{\beta ss}$ were specifically derived by Liu *et al.* [41]. The side slip angle determined by this method is based on vehicle motion states and road conditions, resulting in, to a certain extent, an undesired value in critical situations.

In this study, the yaw rate and side slip angle are independently controlled by decoupling vehicle motion states, and the

eight IWMs possess sufficient capacity to satisfy the control requirements. Therefore, the desired side slip angle in this study is set to zero for a good handling stability. That is

$$\beta_{des} = 0. \tag{17}$$

C. UPPER LAYER CONTROLLER FOR VEHICLE MOTION CONTROL

The upper layer controller is designed to control vehicle motion states to track the desired ones, i.e., the desired longitudinal velocity, desired side slip angle, and desired yaw rate. The three motion states are controlled by the resultant force and moment, i.e., the longitudinal force F_{xc}, lateral force F_{yc}, and yaw moment M_{zc}, which originate from the tire longitudinal force F_{xwij} and lateral force F_{ywij}. Notably, the tire longitudinal force F_{xwij} can be precisely controlled by adjusting the driving or braking torque of electric wheel. However, the tire lateral force F_{ywij} is relatively difficult to control because of the nonlinear cornering characteristics of tires. Especially for a vehicle without active steering equipment, the control of the lateral force F_{ywij} would make the algorithm too complex to apply practically. Thus, in this study, the control variables $\overrightarrow{\mathbf{F}}_{\mathbf{v}}$ of upper controller are selected as the longitudinal force F_{xc}, lateral force F_{yc}, and yaw moment M_{zc}. They originate from the tire longitudinal force F_{xwij} on the tire coordinate frame only, rather than from the tire lateral force F_{ywij}. That is

$$\overrightarrow{\mathbf{F}}_{\mathbf{v}} = \begin{bmatrix} F_{xc} \\ F_{yc} \\ M_{zc} \end{bmatrix} = \begin{bmatrix} \sum_{i=1}^{4} (F_{xwil}\cos\delta_{il} + F_{xwir}\cos\delta_{ir}) \\ \sum_{i=1}^{4} (F_{xwil}\sin\delta_{il} + F_{xwir}\sin\delta_{ir}) \\ \frac{D_b}{2}\sum_{i=1}^{4} (F_{xwir}\cos\delta_{ir} - F_{xwil}\cos\delta_{il}) \end{bmatrix}. \tag{18}$$

Based on the control variables $\overrightarrow{\mathbf{F}}_{\mathbf{v}}$, the dynamics equations (1) to (3) can be rewritten as:

$$m(\dot{v}_x - v_y\omega_z) = F_{xc} - \sum_{i=1}^{4} (F_{ywil}\sin\delta_{il} + F_{ywir}\sin\delta_{ir}) - (mgf_r + 0.5C_D A_f \rho_a v_x^2) + \xi_x \tag{19}$$

$$mv_x(\dot{\beta} + \omega_z) = F_{yc} + \sum_{i=1}^{4} (F_{ywil}\cos\delta_{il} + F_{ywir}\cos\delta_{ir}) + \xi_y \tag{20}$$

$$I_z\dot{\omega}_z = M_{zc} + [\frac{D_b}{2}\sum_{i=1}^{4} (F_{ywil}\sin\delta_{il} - F_{yiwr}\sin\delta_{ir}) + \sum_{i=1}^{2} L_i(F_{ywil} + F_{ywir}) - \sum_{i=3}^{4} L_i(F_{ywil} + F_{ywir})] + \xi_z \tag{21}$$

where ξ_x, ξ_y, and ξ_z represent the nonlinear uncertainties caused by model simplification and the environmental disturbance.

According (19) to (21), the longitudinal velocity, the side slip angle, and the yaw rate can be independently controlled by the longitudinal controlled force F_{xc}, the lateral controlled force F_{yc}, and the controlled yaw moment M_{zc}, respectively. This method simultaneously control the three motion states, without linearizing of the vehicle model and the tire model, which is beneficial to improve the control effectiveness under the extreme conditions.

Because the vehicle motion features nonlinear uncertainties and environmental disturbance, the general linear control algorithms, such as the linear quadratic programing (LQR), are not feasible. As a control method with good effects on nonlinear systems, the sliding mode control (SMC) algorithm improves the system robustness in terms of the nonlinear uncertainties and disturbances. Therefore, the SMC is used to control vehicle motion in this section.

1) LONGITUDINAL VELOCITY CONTROL

The longitudinal velocity controller is designed to determine a longitudinal controlled force to track the desired longitudinal velocity. To eliminate the bias between the measured velocity and the desired velocity, we define the sliding surface as:

$$s_{v_x} = v_x - v_{xdes} \tag{22}$$

To reduce the chattering effects, an exponentially reaching law with a saturation function is defined as:

$$\dot{s}_{v_x} = -\varepsilon_{v_x} sat(s_{v_x}) - k_{v_x} s_{v_x}, \quad \varepsilon_{v_x} > 0,\ k_{v_x} > 0 \tag{23}$$

Based on (19), the longitudinal controlled force for velocity tracking can be deduced as:

$$F_{xc} = \sum_{1}^{4} (F_{ywil}\sin\delta_{il} + F_{ywir}\sin\delta_{ir}) + (mgf_r + 0.5C_D A_f \rho_a v_x^2) + m[\dot{v}_{xdes} - v_y\omega_z - \varepsilon_{v_x} sat(s_{v_x}) - k_{v_x} s_{v_x}] \tag{24}$$

2) SIDE SLIP ANGLE CONTROL

The side slip angle controller is designed to determine a lateral controlled force to track the desired side slip angle. We define the sliding surface as:

$$s_\beta = \beta - \beta_{des} \tag{25}$$

An exponentially reaching law with a saturation function is defined as:

$$\dot{s}_\beta = -\varepsilon_\beta sat(s_\beta) - k_\beta s_\beta, \quad \varepsilon_\beta > 0,\ k_\beta > 0 \tag{26}$$

Based on (20), the lateral controlled force for side slip angle tracking can be derived as:

$$F_{yc} = -\sum_{i=1}^{4} (F_{ywil}\cos\delta_{il} + F_{ywir}\cos\delta_{ir}) + mv_x[\omega_z + \dot{\beta}_{des} - \varepsilon_\beta sat(s_\beta) - k_\beta s_\beta] \tag{27}$$

3) YAW RATE CONTROL

The yaw rate controller is designed to determine a controlled yaw moment to track the desired yaw rate. We define the sliding surface as:

$$s_{\omega_z} = \omega_z - \omega_{zdes} \tag{28}$$

An exponentially reaching law with a saturation function is defined as:

$$\dot{s}_{\omega_z} = -\varepsilon_{\omega_z} sat(s_{\omega_z}) - k_{\omega_z} \cdot s_{\omega_z}, \quad \varepsilon_{\omega_z} > 0,\ k_{\omega_z} > 0 \tag{29}$$

Based on (21), the controlled yaw moment for yaw rate tracking can be deduced as:

$$\begin{aligned} M_{zc} = &-\frac{D_b}{2}\sum_{i=1}^{4}(F_{ywil}\sin\delta_{il} - F_{yiwr}\sin\delta_{ir}) \\ &-\sum_{i=1}^{2} L_i(F_{ywil} + F_{ywir}) \\ &+\sum_{i=3}^{4} L_i(F_{ywil} + F_{ywir}) \\ &+ I_z[\dot{\omega}_{zdes} - \varepsilon_{\omega_z} sat(s_{\omega_z}) - k_{\omega_z} s_{\omega_z}] \end{aligned} \tag{30}$$

Notably, in (23), (26) and (29), the saturation function is defined as:

$$sat(s/\Phi) = \begin{cases} \mathrm{sgn}(s), & if \ \ |s| \geq \Phi \\ s/\Phi, & if \ \ |s| < \Phi \end{cases} \tag{31}$$

D. LOWER LAYER CONTROLLER FOR TORQUE ALLOCATION

The lower layer controller is designed to allocate the electric wheel's torque, including the driving torque and braking torque, to provide the controlled force and moment determined by the upper layer controller. In this paper, the Control Allocation (CA) algorithm, wildly applied in flight control [42], is used to optimize the torque allocation of electric wheels. In addition, an conventional torque allocation method based on rules is intruduced as a comparison.

1) CONTROL-ALLOCATION-BASED CONTROLLER

The control variables $\overrightarrow{\mathbf{F}}_{\mathbf{v}}$, determined by the upper layer controller, are generated by the tire longitudinal force F_{xwij}, which essentially originates from the electric wheel's torque. Based on (18), the relationship between $\overrightarrow{\mathbf{F}}_{\mathbf{v}}$ and F_{xwij} can be expressed as:

$$\vec{\mathbf{F}}_v = \mathbf{B_v}\vec{\mathbf{u}} \tag{32}$$

where

Equation (31) represents a statically indeterminate system, which indicates that the four-axle ground vehicle is an over-actuated system. To achieve optimal handling stability control, an objective function with constraints is established, based on two factors: the tracking precision and the dynamics stability.

To precisely track the desired motion states, the resultant force and moment, generated by the tire longitudinal force $\vec{\mathbf{u}}$, should approximate the controlled variables $\overrightarrow{\mathbf{F}}_{\mathbf{v}}$ as much as possible. Therefore, we define an objective function of the tracking precision:

$$j_1 = \arg\min \left\| W_v(\mathbf{B_v}\vec{\mathbf{u}} - \vec{\mathbf{F}}_{\mathbf{v}}) \right\|^2 \tag{33}$$

where W_v represents a weighting factor matrix for tracking performance, which is defined as:

$$W_v = diag(W_{vF_{xc}}, W_{vF_{yc}}, W_{vM_{zc}}) \tag{34}$$

By adjusting the values of W_{vFxc}, W_{vFyc} and W_{vMzc}, the tracking performance of the longitudinal velocity, the side slip angle, and the yaw rate are controlled, respectively.

In addition, the tire workload rate influences vehicle dynamics stability. In this paper, the longitudinal tire workload rate ρ is defined as:

$$\rho_{ij} = \frac{F_{xwij}}{\mu_{ij}F_{zij}} \tag{35}$$

where the denominator $(\mu_{ij}F_{zij})$ represents the maximum tire adhesion force. The smaller the tire workload rate, the higher the stability margin. Therefore, we define another objective function of the handling stability as:

$$j_2 = \arg\min \left\| W_u\vec{\mathbf{u}} \right\|^2 \tag{36}$$

where W_u is a weighting matrix with adjustable factors C_{ij} $(i = 1, 2, 3, 4;\ j = l, r)$ for adjusting tire workload rate, shown as:

$$W_u = diag\left(\frac{C_{1l}}{\mu_{1l}F_{z1l}}, \frac{C_{1r}}{\mu_{1r}F_{z1r}}, \frac{C_{2l}}{\mu_{2l}F_{z2l}}, \frac{C_{2r}}{\mu_{2r}F_{z2r}}, \cdots \right.$$
$$\left. \frac{C_{3l}}{\mu_{3l}F_{z3l}}, \frac{C_{3r}}{\mu_{3r}F_{z3r}}, \frac{C_{4l}}{\mu_{4l}F_{z4l}}, \frac{C_{4r}}{\mu_{4r}F_{z4r}} \right) \tag{37}$$

The tire force F_{xwij} is restrained by the electric wheel torque capability and the friction ellipse constraints.

According to the objective functions of the tracking precision and handling stability, a comprehensive objective function of torque allocation with constraints is established as:

$$\begin{cases} J = \arg\min\left(\gamma \left\| W_v\left(Bu - v\right)\right\|^2 + \left\| W_u u\right\|^2\right) \\ s.t. \begin{cases} -\sqrt{\left(\mu_{ij}F_{zij}\right)^2 - F_{ywij}^2} \leq F_{xwij} \leq \sqrt{\left(\mu_{ij}F_{zij}\right)^2 - F_{ywij}^2} \\ \dfrac{-T_{m\max}i_g - T_{b\max}}{R_w} \leq F_{xwij} \leq \dfrac{T_{m\max}i_g}{R_w} \end{cases} \end{cases} \tag{38}$$

where γ is the weighting factor. The optimal solution $\boldsymbol{F}^*_{\boldsymbol{xwij}}$ of (38) can be solved by using the Sequential Quadratic Programming (SQP) algorithm, which is widely used for optimization issues with constraints, and features a good global and super-linear convergence [16], [43].

Once the optimal tire forces $\boldsymbol{F}^*_{xwij}$ are solved, according to the relationship between the driving torque and the braking torque in the electric wheel, as shown in (10) and (11),

the PMSM torque T_{mij} and the braking torque T_{bij} can be allocated as following rules:

If

$$-T_{\max mij} i_g \le F^*_{xwij} R_w \le T_{\max mij} i_g, \tag{39}$$

then

$$T_{mij} = F^*_{xwij} R_w / i_g, \quad T_{bij} = 0; \tag{40}$$

Otherwise

$$T_{mij} = -T_{\max mij}, \quad T_{bij} = -(F^*_{xwij} R_w + T_{\max mij} i_g). \tag{41}$$

2) RULE-BASED CONTROLLER

For centralized powered vehicles, the handling stability control is mainly achieved by adjusting the braking system torque. The braking strategy is as follows [10]: when the steering yaw moment must be increased, braking the inner-rear wheel is the top priority, and when the steering yaw moment needs to be reduced, braking the outer-front wheel is the top priority.

Based on above braking strategy, a rule-based braking torque allocation method is utilized to compare to the CA-based method proposed in this paper. As shown in Fig. 8, if vehicle performs understeer, the inner-side wheels are braked; and if vehicle preforms oversteer, the outer-side wheels are braked. A single wheel is difficult to satisfy the large value of the required yaw moment ∇M_{zb} for multi-axle vehicles. Thus, we allocate the braking torque to the braking-side wheels as follows: the top priority wheel provides 50% of the total braking torque, and the other wheels on the same side 25%, 15%, and 10%, respectively.

According to the above rules on braking torque allocation, we can determine the braking torque of each electric wheel as follows.

(1) If the vehicle is making a left turn with understeer, validated by $\omega_{zdes} > 0$ and $|\omega_z| < |\omega_{zdes}|$, the left-side wheels are braked, and the wheel marked as *4l* is the top priority wheel. The braking force of the four left-side wheels is calculated by:

$$\begin{cases} \nabla M_{zb} = \dfrac{D_b}{2} \displaystyle\sum_{i=1}^{4} (F_{bil} \cos \delta_{il}) - \sum_{i=1}^{4} (L_i F_{bil} \sin \delta_{1l}) \\ F_{b1l} = 0.1F_b; \quad F_{b2l} = 0.15F_b; \\ F_{b3l} = 0.25F_b; \quad F_{b4l} = 0.5F_b \end{cases} \tag{42}$$

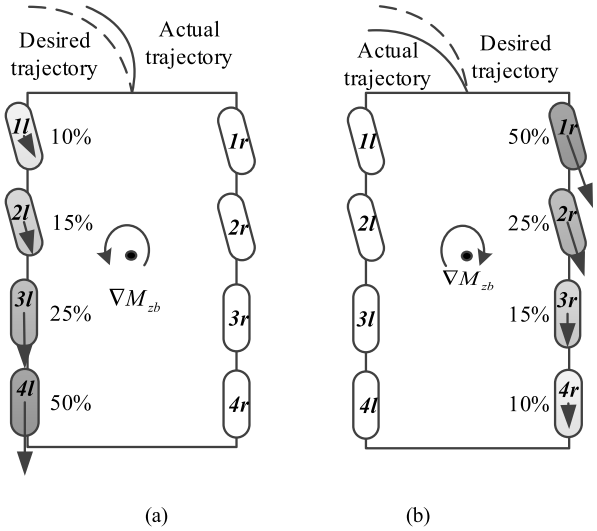

FIGURE 8. Rule-based torque allocation. (a) Understeer situation. (b) Oversteer situation.

(2) If the vehicle is making a left turn with oversteer, validated by $\omega_{zdes} > 0$ and $|\omega_z| > |\omega_{zdes}|$, the right-side wheels are braked, and the wheel marked as *1r* is the top priority wheel. The braking force of the four right-side wheels is calculated by:

$$\begin{cases} \nabla M_{zb} = \dfrac{D_b}{2} \displaystyle\sum_{i=1}^{4} (F_{bir} \cos \delta_{ir}) + \sum_{i=1}^{4} (L_i F_{bir} \sin \delta_{1r}) \\ F_{b1r} = 0.5F_b; \quad F_{b2r} = 0.25F_b; \\ F_{b3r} = 0.15F_b; F_{b4r} = 0.1F_b \end{cases} \tag{43}$$

(3) If the vehicle is making a right turn with understeer, validated by $\omega_{zdes} < 0$ and $|\omega_z| < |\omega_{zdes}|$, the right-side wheels are braked, and the wheel marked as *4r* is the top priority wheel. The braking force of the four right-side wheels is calculated by:

$$\begin{cases} \nabla M_{zb} = \dfrac{D_b}{2} \displaystyle\sum_{i=1}^{4} (F_{bir} \cos \delta_{ir}) - \sum_{i=1}^{4} (L_i F_{bir} \sin \delta_{1r}) \\ F_{b1r} = 0.1F_b; \quad F_{b2r} = 0.15F_b; \\ F_{b3r} = 0.25F_b; \quad F_{b4r} = 0.5F_b \end{cases} \tag{44}$$

$$\begin{cases} \vec{\mathbf{F}}_v = [F_{xc} \quad F_{yc} \quad M_{zc}]^T \\ \vec{\mathbf{u}} = [F_{xw1l} \quad F_{xw1r} \quad F_{xw2l} \quad F_{xw2r} \quad F_{xw3l} \quad F_{xw3r} \quad F_{xw4l} \quad F_{xw4r}]^T \\ \mathbf{B_v} = \begin{bmatrix} \cos\delta_{1l} & \cos\delta_{1r} & \cos\delta_{2l} & \cos\delta_{2r} & 1 & 1 & 1 & 1 \\ \sin\delta_{1l} & \sin\delta_{1r} & \sin\delta_{2l} & \sin\delta_{2r} & 0 & 0 & 0 & 0 \\ \left(\begin{matrix} -\frac{D_b}{2}\cos\delta_{1l} \\ +L_1 \sin\delta_{1l} \end{matrix}\right) & \left(\begin{matrix} \frac{D_b}{2}\cos\delta_{1r} \\ +L_1 \sin\delta_{1r} \end{matrix}\right) & \left(\begin{matrix} -\frac{D_b}{2}\cos\delta_{2l} \\ +L_2 \sin\delta_{2l} \end{matrix}\right) & \left(\begin{matrix} \frac{D_b}{2}\cos\delta_{2r} \\ +L_2 \sin\delta_{2r} \end{matrix}\right) & -\frac{D_b}{2} & \frac{D_b}{2} & -\frac{D_b}{2} & \frac{D_b}{2} \end{bmatrix} \end{cases}$$

(4) If the vehicle is making a right turn with oversteer, validated by $\omega_{zdes} < 0$ and $|\omega_z| > |\omega_{zdes}|$, the left-side wheels are braked, and the wheel marked as *1l* is the top priority wheel. The braking force of the four left-side wheels is calculated by:

$$\begin{cases} \nabla M_{zb} = \dfrac{D_b}{2}\sum_{i=1}^{4}(F_{bil}\cos\delta_{ir}) + \sum_{i=1}^{4}(L_i F_{bil}\sin\delta_{1l}) \\ F_{b1l} = 0.5F_b; \quad F_{b2l} = 0.25F_b; \\ \quad F_{b3l} = 0.15F_b; \quad F_{b4l} = 0.1F_b \end{cases} \tag{45}$$

By using (42) to (45), we can calculate the braking force F_{bij} $(i = 1, 2, 3, 4; j = i, l)$ of each wheel. Finally, the braking torque T_{bij} $(i = 1, 2, 3, 4; j = i, l)$ is determined by:

$$T_{bij} = F_{bij} \cdot R_w. \tag{46}$$

IV. SIMULATION AND TEST VALIDATION

In this section, a simulation based on the Matlab/Simulink software and a hardware-in-loop (HIL) test based on the dSPACE platform are performed to validate the effectiveness of the proposed control strategy. The vehicle basic parameters, as shown in table 1, are obtained from a full-sized four-axle HEGV driven by IWMs, as shown in Fig. 9.

TABLE 1. The basic parameters of the ground vehicle.

Variables	Notation	Value	Unit
Vehicle mass	m	21000	kg
Vehicle inertia Moment around z axis	I_z	36000	kg·m^2
Distance from the mass center to the first axle	L_1	2.23	m
Distance from the mass center to the second axle	L_2	0.81	m
Distance from the mass center to the third axle	L_3	1.19	m
Distance from the mass center to the fourth axle	L_4	2.61	m
Wheel-track	D_b	2.6	m
Tire mass (including the IWM)	m_w	400	kg
Tire inertia moment around y^w axis	I_w	150	kg·m^2
Wheel effective radius	R_w	0.59	m
Transmission ration of the wheel-side reducer	i_g	11	-
Transmission ration of the steering mechanism	i_{sw}	20	-

A. FISH-HOOK STEERING SIMULATION

In this simulation, the tire-road adhesion coefficient is set to 0.4, and the vehicle desired velocity is set to 50 km/h. The fish-hook steering inputs, as shown in Fig. 10 (a), include a pulse steering (0-2s) and a step steering (2-10s), in which δ_{sw} represents the steering wheel angle, and δ_{ij} represents the four front directive tires' steering angles.

FIGURE 9. Full-sized four-axle HEGV driven by IWMs.

Fig. 10 (b) shows the trajectory tracking results of the control schemes. Both of the CA-based control and the rule-based control improve the vehicle tracking performance. In the enlarged view, the rule-based control makes vehicle a little understeer in the pulse string period (0-2s), and oversteer in the step steering period (2-10s). By contrast, the CA-based control performs best in trajectory tracking in the whole process. Fig. 10 (c) presents the desired yaw rate tracking performance of the control schemes. It can be seen that the vehicle without control fails to track the desired yaw rate, indicating the vehicle is instability in this situation. The vehicle under the rule-based control tracks the desired yaw rate with large overshoots and a long settling time in 1-3s period. The vehicle under the CA-based control stably tracks the desired yaw rate with high precision in the whole process, resulting in the excellent trajectory tracking performance. Fig. 10 (d) compares the phase plane of the side slip angle under the control schemes. Compared to the vehicle without control, the vehicles' side slip angle under the CA-based control and the rule-based control eventually converge in the phase plane. Especially, the side slip angle and its change rate under the CA-based control are smaller than those under the rule-based control, meaning that the CA-based control results in better vehicle stability.

Fig. 11 shows the torque allocation of electric wheels, including the PMSM torque and braking torque, under the CA-based control. It can be seen that torque is allocated to the different PMSMs and brakes. Under the pulse steering maneuver (0-2s), torque from the four front wheels is dominated. This is because the four front wheels contribute to more lateral force and yaw moment as steering wheels. As shown in Fig. 11 (a) and (b), when the PMSM torque reaches the constraint boundary, the corresponding braking torque compensates. Under the step steering maneuver (2-10s), torque is primarily allocated to the right-side PMSMs, as shown in Fig. 11 (a) and (c), to ensure vehicle handing stability. Because the torques is within PMSMs' capacity, no braking torque occurs in this period, as shown in Fig. 11 (b) and (d).

Fig. 12 shows the braking torque allocation with the rule-based control. During the pulse steering maneuver (0-2s), the braking torque dramatically shifts among the wheels. During the step steering maneuver (2-10s), the braking torque

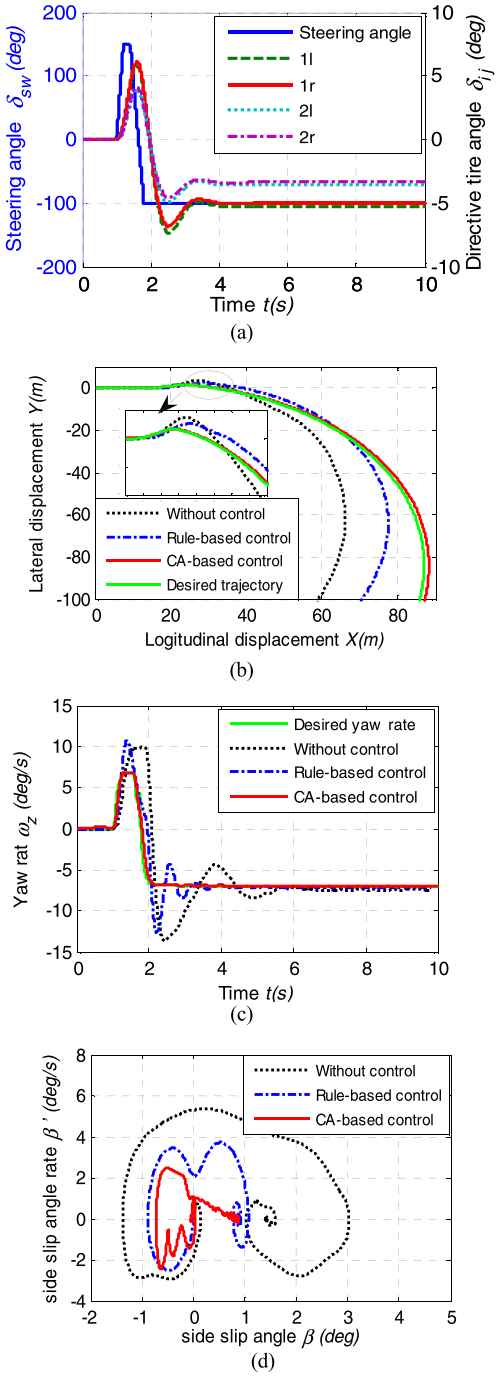

FIGURE 10. Vehicle motion states. (a) Fish-hook steering inputs. (b) Trajectory tracking. (c) Yaw rate. (d) Side slip angle and change rate.

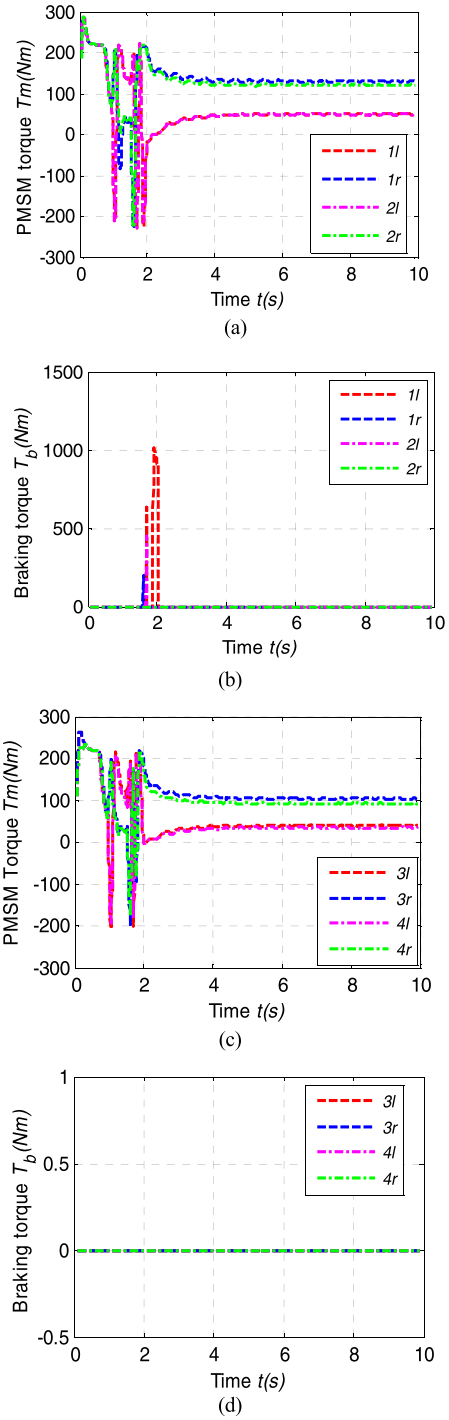

FIGURE 11. Torque from PMSMs and brakes in control allocation (CA)-based control. (a) Torque of the four front PMSMs. (b) Braking torque of the four front wheels. (c) Torque of the four rear PMSMs. (d) Braking torque of the four rear wheels.

is mostly output from the two front right-side wheels for generating the controlled yaw moment to overcome vehicle oversteering.

Fig. 13 displays the tire workload rate under the two control schemes. During the step steering maneuver, the workload rates of the right side tires are larger than that of the left side tires because the steering yaw moment is primarily generated from the torque of right side tires. In comparison, the tire workload rates under the CA-based control are lower and more stable, indicating that the vehicle is more stable margin and has better handling stability.

B. VEHICLE CONTROLLER IN LOOP TEST

To validate the reliability and real-time performance of the proposed CA-based control strategy, a hardware-in-loop

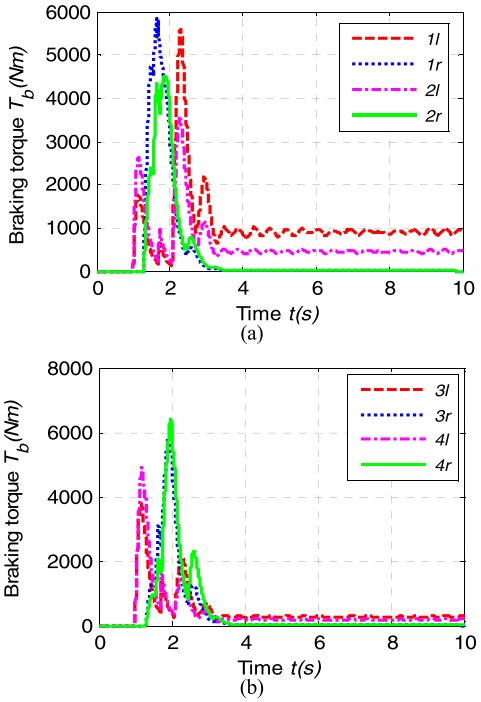

FIGURE 12. Torque from brakes with rule-based control. (a) Braking torque of the four front wheels. (b) Braking torque of the four rear wheels.

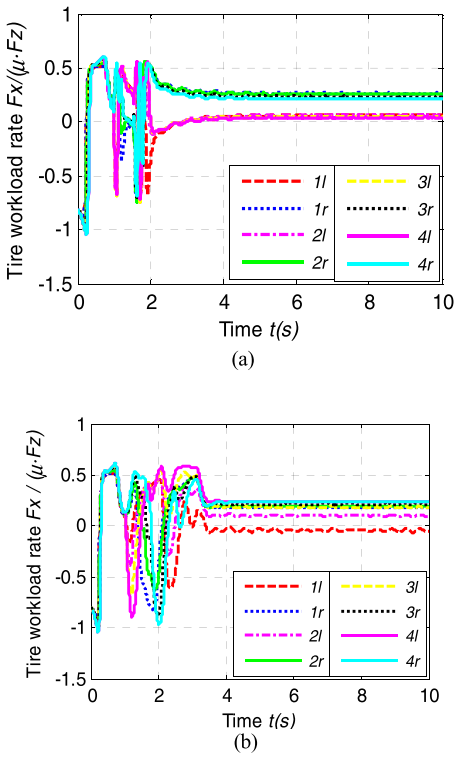

FIGURE 13. Tire work load rate in (a) CA-based control, and (b) rule-based control.

(HIL) test based on the dSPACE platform was conducted. As shown in Fig. 14 (a), the vehicle model is downloaded to the real-time platform dSPACE autobox, and the proposed

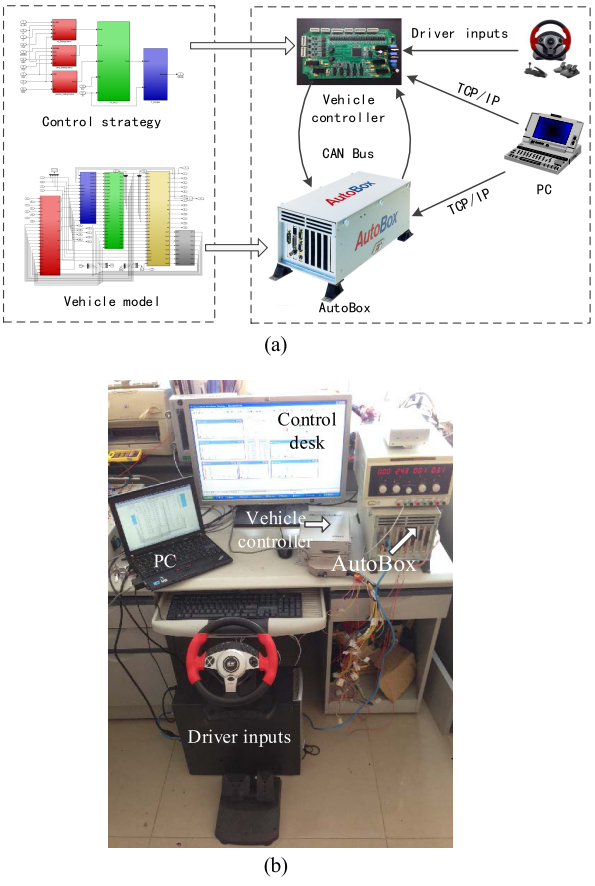

FIGURE 14. Hardware-in-loop (HIL) architecture and test platform. (a) dSPACE-based HIL architecture. (b) HIL test platform.

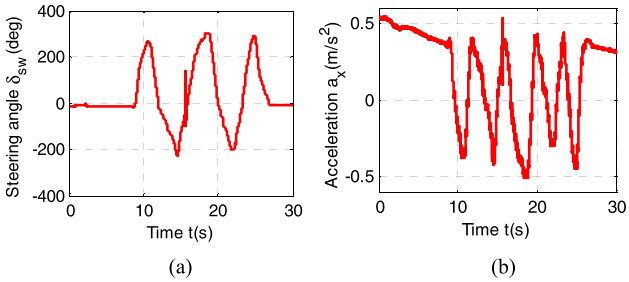

FIGURE 15. Driver inputs. (a) Steering wheel angle. (b) Longitudinal acceleration.

control strategy is run on an electronic control unit (ECU) hardware. The real-time platform communicates with the ECU controller through a Controller Area Network (CAN) bus. Fig. 14 (b) displays the HIL test platform. The ECU in the HIL is developed based on the MC9S12DP256 chip, which is one of the Freescale Semiconductor's HCS12 family of microcontrollers.

In this HIL test, the driver inputs, as shown in Fig. 15, include the vehicle steering angle and acceleration, based on the steering wheel and the pedal, respectively. The tire-road coefficient is set to 0.4 with an initial velocity of 70 km/h. Fig. 15(a) presents the steering input, which is

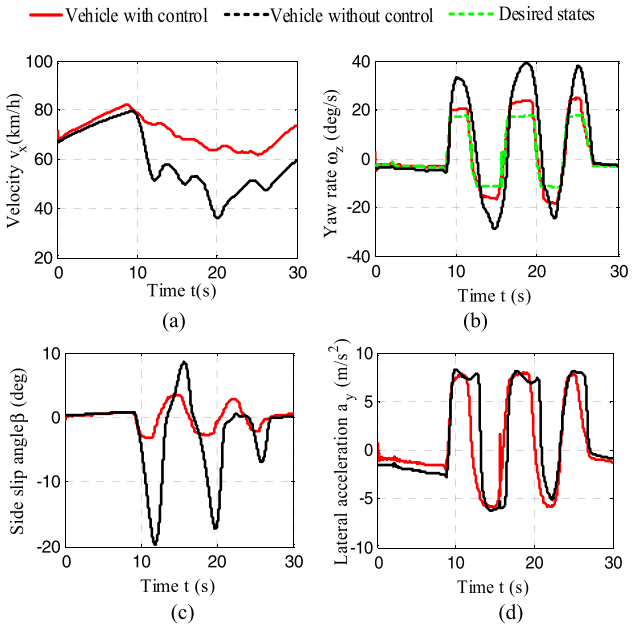

FIGURE 16. Vehicle motion states. (a) Longitudinal velocity. (b) Yaw rate. (c) Side slip angle. (d) Lateral acceleration.

approximately a sine wave. In the test, we attempted to maintain a constant velocity, but the acceleration fluctuated within a certain range, as shown in Fig. 15 (b).

Fig. 16 shows the vehicle motion states in the HIL test. Compared to the uncontrolled vehicle, the vehicle with CA-based control maintains the velocity better, and exhibits better performance in tracking the desired yaw rate and side slip angle, indicating the proposed control strategy effectively improves vehicle motion stability. However, as shown in Fig. 16 (b), compared to the software simulation result in Fig. 10 (c), some deviation between the controlled motion states and the desired ones occurs. That is mainly because the algorithms running in the controller are based on a fixed step solver. And, the periodic transmission mode of the CAN bus results in a certain information transmit lag. In addition, the ECU adopted in the HIL is not efficient in the floating point arithmetic due to the limited memory size. In the HIL test, the objective function was solved offline, and then the optimal solutions were tabulated and loaded into the memory flash of ECU for looking up online. These reasons lead to the deviation between the controlled motion states and the desired ones.

Fig. 17 demonstrates the torque allocation in the electric wheels. As shown in Fig. 17 (a) and (c), the PMSM torque is assigned based on the proposed CA-based control. When the PMSM torque reaches the constraint boundary, the braking torque compensates it, as shown in Fig. 17 (b) and (d). The PMSMs and the braking system coordinate to output the torque based on the proposed control strategy with good performance in real-time and reliability.

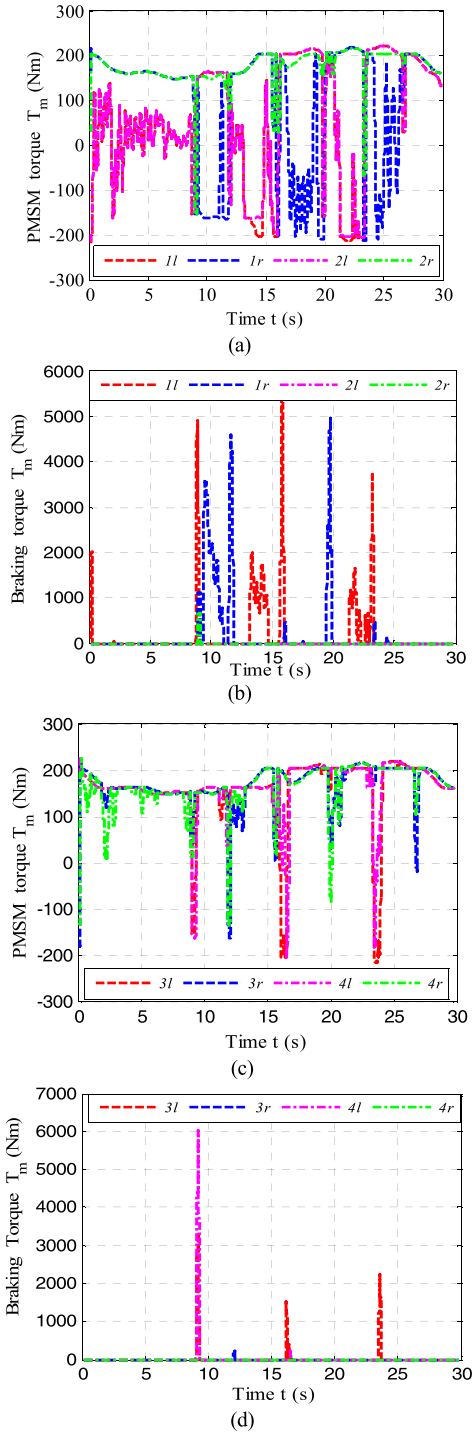

FIGURE 17. Torque from PMSMs and brakes of vehicle with control. (a) Torque of the four front PMSMs. (b) Braking torque of the four front wheels. (c) Torque of the four rear PMSMs. (d) Braking torque of the four rear wheels.

V. CONCLUSIONS

This paper presents an optimization control strategy for a four-axle HEGV driven by IWMs to improve the handling stability. The key conclusions include:

(1) The architecture of a four-axle HEGV driven by IWMs was introduced. Focusing on improving vehicle handling

stability, a nonlinear vehicle dynamics model with 11 DOFs was established. By using the ''Magic Formula'' tire model, the vehicle dynamics model could precisely reflect the vehicle characteristics of the longitudinal, lateral and yaw motion.

(2) To improve vehicle handling stability, a hierarchical optimization control strategy was proposed. In the upper layer controller, by using the nonlinear sliding mode control (SMC) method, the controlled force and yaw moment were determined to independently control the vehicle motion states to track the desired states. In the lower layer controller, the controlled force and moment, determined in the upper controller, were realized by assigning the actuators torque. Considering the motor torque capability, the tire work load rate, and the road adhesion as constraints, we established an objective function. The control allocation (CA) method, based on the Sequential Quadratic Programming (SQP) algorithm, was used to solve the objective function for the optimal torque allocation. In addition, a rule-based torque allocation method was introduced for comparison.

(3) A software simulation and a HIL test were conducted to validate the effectiveness of the proposed control strategy. The simulation results of the fish-hook steering showed that, the proposed control strategy exhibited excellent performance for vehicle handling stability. Furthermore, the HIL test results demonstrated that the proposed strategy had the capability of reliability for real-time implementation.

REFERENCES

[1] X. Wu, X. Hu, S. Moura, X. Yin, and V. Pickert, ''Stochastic control of smart home energy management with plug-in electric vehicle battery energy storage and photovoltaic array,'' *J. Power Sources*, vol. 333, pp. 203–212, Nov. 2016.

[2] X. Tang, W. Yang, X. Hu, and D. Zhang, ''A novel simplified model for torsional vibration analysis of a series-parallel hybrid electric vehicle,'' *Mech. Syst. Signal Process.*, vol. 85, pp. 329–338, Feb. 2017.

[3] L. Boulon, D. Hissel, A. Bouscayrol, O. Pape, and M.-C. Pera, ''Simulation model of a military HEV with a highly redundant architecture,'' *IEEE Trans. Veh. Technol.*, vol. 59, no. 6, pp. 2654–2663, Jul. 2010.

[4] M. Velardocchia and E. Rondinelli, ''Design and development of an in-hub motors hybrid vehicle for military applications,'' SAE Tech. Paper 2010-01-0659, Apr. 2010.

[5] Y. J. Huang, H. Wang, A. Khajepour, H. W. He, and J. Ji, ''Model predictive control power management strategies for HEVs: A review,'' *J. Power Sources*, vol. 341, pp. 91–106, Feb. 2017.

[6] Z. Y. Chen, R. Xiong, C. Wang, and J. Cao, ''An on-line predictive energy management strategy for plug-in hybrid electric vehicles to counter the uncertain prediction of the driving cycle,'' *Appl. Energy*, vol. 185, no. 2, pp. 1663–1672, Jan. 2017.

[7] C. M. Martinez, X. Hu, D. Cao, E. Velenis, B. Gao, and M. Wellers, ''Energy management in plug-in hybrid electric vehicles: Recent progress and a connected vehicles perspective,'' *IEEE Trans. Veh. Technol.*, vol. 66, no. 6, pp. 4534–4549, Jun. 2017.

[8] C. Sun, X. Hu, S. J. Moura, and F. Sun, ''Velocity predictors for predictive energy management in hybrid electric vehicles,'' *IEEE Trans. Control Syst. Technol.*, vol. 23, no. 3, pp. 1197–1204, May 2015.

[9] X. Hu, H. Wang, and X. Tang, ''Cyber-physical control for energy-saving vehicle following with connectivity,'' *IEEE Trans. Ind. Electron.*, vol. 64, no. 11, pp. 8578–8587, Nov. 2017.

[10] W. Kim, K. Yi, and J. Lee, ''An optimal traction, braking, and steering coordination strategy for stability and manoeuvrability of a six-wheel drive and six-wheel steer vehicle,'' *Proc. Inst. Mech. Eng., D, J. Autom. Eng.*, vol. 226, pp. 3–22, Sep. 2012.

[11] Y. Gao, Y. Shen, X. Liu, and X. Wei, ''Stability control for eight-axle independent in-wheel motor drive vehicle considering the effects of steering angle,'' *Autom. Eng.*, vol. 38, no. 4, pp. 403–409 and 472, Apr. 2016.

[12] Y. Chen, X. Li, C. Wiet, and J. Wang, ''Energy management and driving strategy for in-wheel motor electric ground vehicles with terrain profile preview,'' *IEEE Trans Ind. Informat.*, vol. 10, no. 3, pp. 1938–1947, Aug. 2014.

[13] R. Wang, C. Hu, F. Yan, and M. Chadli, ''Composite nonlinear feedback control for path following of four-wheel independently actuated autonomous ground vehicles,'' *IEEE Trans. Intell. Transp. Syst.*, vol. 17, no. 7, pp. 2063–2074, Mar. 2016.

[14] M. Liu, F. Gu, and Y. Zhang, ''Ride comfort optimization of in-wheel-motor electric vehicles with in-wheel vibration absorbers,'' *Energies*, vol. 10, no. 10, p. 1647, Oct. 2017.

[15] Z. Yu, Y. Feng, and L. Xiong, ''Review on vehicle dynamics control of distributed drive electric vehicle,'' *J. Mech. Eng.*, vol. 49, no. 8, pp. 105–114, Apr. 2013.

[16] Z. Wang, Y. Wang, L. Zhang, and M. Liu, ''Vehicle stability enhancement through hierarchical control for a four-wheel-independently-actuated electric vehicle,'' *Energies*, vol. 10, no. 7, p. 947, Jul. 2017.

[17] A. T. Van Zanten, R. Erhardt, A. Lutz, W. Neuwald, and H. Bartels, ''Simulation for the development of the bosch-VDC,'' SAE Tech. Paper 960486, 1996.

[18] H. Fujimoto, A. Tsumasaka, and T. Noguchi, ''Vehicle stability control of small electric vehicle on snowy road,'' *Rev. Autom. Eng.*, vol. 27, no. 2, pp. 279–286, Feb. 2006.

[19] H. Yu and M. Huang, ''Potential energy analysis and limit cycle control for dynamics stability of in-wheel driving electric vehicle,'' in *Proc. IEEE Vehicle Power Propuls. Conf.*, Harbin, China, Sep. 2008, pp. 1–8.

[20] W. Chen, X. Liu, H. Huang, and H. Yu, ''Research on side slip angle dynamic boundary control for vehicle stability control considering the impact of road surface,'' *J. Mech. Eng.*, vol. 48, no. 14, pp. 112–118, Jul. 2012.

[21] F. Tahami, R. Kazemi, and S. Farhanghi, ''A novel driver assist stability system for all-wheel-drive electric vehicles,'' *IEEE Trans. Veh. Technol.*, vol. 52, no. 3, pp. 683–692, May 2003.

[22] D. Kim, S. Hwang, and H. Kim, ''Vehicle stability enhancement of four-wheel-drive hybrid electric vehicle using rear motor control,'' *IEEE Trans. Veh. Technol.*, vol. 57, no. 2, pp. 727–735, Mar. 2008.

[23] V. Ivanov and D. Savitski, ''Systematization of integrated motion control of ground vehicles,'' *IEEE Access*, vol. 3, pp. 2080–2099, 2015.

[24] A. Jackson, D. Crolla, A. Woodhouse, and M. Parsons, ''Improving performance of a 6×6 off-road vehicle through individual wheel control,'' SAE Tech. Paper 2002-01-0968, 2002.

[25] J. N. Wang, Q. N. Wang, C. X. Song, L.-Q. Jin, and C. J. Hu, ''Co-simulation and test of differential drive assist steering control system for four-wheel electric vehicle,'' *Trans. Chin. Soc. Agricult. Mach.*, vol. 41, no. 6, pp. 7–13, Jun. 2010.

[26] J. Wang and R. G. Longoria, ''Coordinated and reconfigurable vehicle dynamics control,'' *IEEE Trans. Control Syst. Technol.*, vol. 17, no. 3, pp. 723–732, May 2009.

[27] W. Kim, K. Yi, and J. Lee, ''Drive control algorithm for an independent 8 in-wheel motor drive vehicle,'' *J. Mech. Sci. Technol.*, vol. 25, no. 6, pp. 1573–1581, Jun. 2011.

[28] Q. Wang, J. Goyal, B. Ayalew, and A. Singh, ''Control allocation for multi-axle hub motor driven land vehicles with active steering,'' *SAE Int. J. Alternative Power*, vol. 5, no. 2, pp. 338–347, Aug. 2016.

[29] H. Zhao, B. Gao, B. Ren, H. Chen, and W. Deng, ''Model predictive control allocation for stability improvement of four-wheel drive electric vehicles in critical driving condition,'' *IET Control Theory Appl.*, vol. 9, no. 18, pp. 2688–2696, Dec. 2015.

[30] L. Xiong, G. W. Teng, Z. P. Yu, W. X. Zhang, and Y. Feng, ''Novel stability control strategy for distributed drive electric vehicle based on driver operation intention,'' *Int. J. Autom. Technol.*, vol. 17, no. 4, pp. 651–663, Jun. 2016.

[31] L. De Novellis, A. Sorniotti, and P. Gruber, ''Wheel torque distribution criteria for electric vehicles with torque-vectoring differentials,'' *IEEE Trans. Veh. Technol.*, vol. 63, no. 4, pp. 1593–1602, May 2014.

[32] S. T. H. Jansen, P. W. A. Zegelaar, and H. B. Pacejka, ''The influence of in-plane tyre dynamics on ABS braking of a quarter vehicle model,'' *Vehicle Syst. Dyn.*, vol. 32, nos. 2–3, pp. 249–261, Aug. 1999.

[33] E. Bakker, L. Nyborg, and H. B. Pacejka, ''Tyre modelling for use in vehicle dynamics studies,'' SAE Tech. Paper 870421, 1987.

[34] M. K. Aripin, Y. M. Sam, K. A. Danapalasingam, K. Peng, N. Hamzah, and M. F. Ismail, ''A review of active yaw control system for vehicle handling and stability enhancement,'' *Int. J. Veh. Technol.*, vol. 2014, Jun. 2014, Art. no. 437515, doi: 10.1155/2014/437515.

[35] A. Higuchi and Y. Saitoh, "Optimal control of four wheel steering vehicle," *Vehicle Syst. Dyn.*, vol. 22, nos. 5–6, pp. 397–410, Sep./Nov. 1993.
[36] R. Marino and S. Scalzi, "Asymptotic sideslip angle and yaw rate decoupling control in four-wheel steering vehicles," *Vehicle Syst. Dyn.*, vol. 48, no. 9, pp. 999–1019, 2010.
[37] S.-J. An, K. Yi, G. Jung, K. I. Lee, and Y.-W. Kim, "Desired yaw rate and steering control method during cornering for a six-wheeled vehicle," *Int. J. Autom. Technol.*, vol. 9, no. 2, pp. 173–181, Apr. 2008.
[38] S. Yu, J. Wang, Y. Wang, and H. Chen, "Disturbance observer based control for four wheel steering vehicles with model reference," *IEEE/CAA J. Autom. Sinica*, to be published, doi: 10.1109/JAS.2016.7510220.
[39] M. Nagai, Y. Hirano, and S. Yamanaka, "Integrated control of active rear wheel steering and direct yaw moment control," *Vehicle Syst. Dyn.*, vol. 27, pp. 357–370, Jun. 1997.
[40] L. Li, G. Jia, J. Chen, H. Zhu, D. Cao, and J. Song, "A novel vehicle dynamics stability control algorithm based on the hierarchical strategy with constrain of nonlinear tyre forces," *Vehicle Syst. Dyn.*, vol. 53, no. 8, pp. 1093–1116, Aug. 2015.
[41] M. Liu, C. Zhang, R. Zhang, and Z. Wang, "Research on steady and transient characteristics of 4-axle vehicle handling," in *Proc. IEEE Transp. Electrif. Conf.*, Beijing, China, Aug. 2014, pp. 1–6.
[42] O. Harkegard and S. T. Glad, "Resolving actuator redundancy—Optimal control vs. control allocation," *Automatica*, vol. 41, no. 1, pp. 137–144, Jan. 2005.
[43] O. Harkegard, "Dynamic control allocation using constrained quadratic programming," *J. Guid., Control, Dyn.*, vol. 27, no. 6, pp. 1028–1034, Nov./Dec. 2004.

MINGCHUN LIU received the B.S. degree in electromechanical engineering, the M.S. degree, and the Ph.D. degree in mechanical engineering from the Beijing Institute of Technology, Beijing, China, in 2009, 2010, and 2015, respectively.

Since 2015, he has been an Assistant Professor with the School of Mechatronics Engineering, Nanchang University. Since 2017, he has been a Post-Doctoral Researcher with the Department of Mechanical and Aerospace Engineering, The Ohio State University, Columbus, OH, USA. His research interests include the electric vehicle system integration, vehicle system dynamics modeling and control, and vehicle control system development.

JUHUA HUANG received the B.S. degree in mechanical engineering from Jiangxi Technology University, Nanchang, China, in 1984, and the M.S. degree and the Ph.D. degree in material processing engineering from Nanchang University, Nanchang, in 1993 and 1998, respectively.

Since 1998, she has been a Professor with the School of Mechatronics Engineering, Nanchang University. Her main research interests include vehicle system dynamics control and electric vehicle design.

MING CAO received the B.S. degree in software engineering and the M.S. degree in vehicle engineering from Nanchang University, Nanchang, China, in 2009 and 2012, respectively.

Since 2012, he has been an Assistant Professor with the School of Mechatronics Engineering, Nanchang University and Jiangxi Engineering Research Center of Vehicle Electronics. Since 2017, he has been a Visiting Scholar with The University of Kansas, Lawrence, KA, USA. His main research interests include battery management system in electric vehicle and vehicle electrical control.